

Inferring Pore Size and Network Structure from Sorption Hysteresis

Matthew B. Pinson, Hamlin M. Jennings, and Martin Z. Bazant
Massachusetts Institute of Technology

(Dated: February 17, 2014)

Sorption experiments are widely used to infer the pore size distribution of a mesoporous material. We present a simple model that explains the hysteresis observed on desorption in such experiments. The model is based on well-established relationships between the radius of a pore and the partial pressure at which it will fill, but additionally describes the connectivity of the pore network. The model is able to explain both primary and scanning sorption isotherms for a range of materials with wide pore size distributions, such as cement paste and dental enamel. It allows quantification of the prevalence of macropores in the material, even though these pores are never filled during the sorption experiments. A distinct bump in the desorption isotherms is attributed to spinodal decomposition (or cavitation) at a partial pressure that depends on temperature, and experiments across a range of sorbents and sorbates are consistent with a universal scaling.

I. INTRODUCTION

The properties of a porous material, such as strength, permeability and hydrodynamic dispersion, depend on the structure of both solid and pore. These microstructures can be difficult to characterize experimentally, especially due to the wide range of length scales, which can extend below one nanometer. A standard characterisation approach is vapor sorption, in which the partial pressure of a sorbate is varied and the sorbed mass (or the intensity of a nuclear magnetic resonance signal [1]) measured. In principle, such measurements enable quantification of the internal surface area, the pore size distribution, and to some extent the connectivity of the pore network.

One difficulty in the interpretation of sorption isotherms is the widely-observed hysteresis between adsorption and desorption isotherms [2]. The dominant cause of sorption hysteresis in many materials is that some pores remain full below the partial pressure at which the empty state is thermodynamically favored, because they lack the connection with the vapor phase that is necessary to nucleate the liquid to vapor transition. This is frequently known as “pore blocking” [3] [4], but we avoid this term because it has the potential to mislead by suggesting a dynamic effect, whereas in fact a metastable state is achieved.

Theoretical models of this hysteresis have been developed, applicable to certain cases but not universally. Mason [5] proposed a model of pores connected by windows, each with a characteristic radius drawn from a distribution [6]. Parlar and Yortsos [7] extended this model to more completely describe the case of scanning isotherms. Seaton [8] applied the model to the calculation of the average coordination number of pores in various materials, while Tanev and Vlaev [3] considered the relationship between assumptions about the pore shape and the corresponding hysteresis loop.

These previous publications share a strong focus on the percolation threshold determined from desorption data, but this makes them inapplicable to the case where the pore size distribution is so broad that an extensive num-

ber of macropores remains empty even at the highest experimentally accessible partial pressures. A better understanding of the prevalence of large and small pores and how they are connected would be beneficial to the modeling of transport in porous media [9], since transport processes are much faster in larger pores. Such transport modeling is applicable to a wide variety of problems, including creep and corrosion in concrete [10], capture of carbon dioxide in sorbents such as zeolites or activated carbon [11], and shale gas extraction [12]. Here we present a model that is able to capture the effect of large as well as small pores, and hence provide information about the entire pore structure.

II. MODEL

A. Adsorption and insertion

In addition to capillary condensation, the sorbate can be sorbed by a material through adsorption on its internal surfaces, and in many cases [13] [14] by other mechanisms such as insertion into the solid material that makes up the porous structure. In order to use an analysis of capillary condensation to determine the pore structure, sorption due to these mechanisms must be subtracted from the total. The quantitative details of these mechanisms are material-specific and presumably rather complicated, and a correct treatment must account for effects of discreteness [15]. We avoid these complications by using the following simple approximation that is sufficient to enable a reasonably accurate calculation of the capillary condensed mass as a function of partial pressure.

The classical equation for surface adsorption is the Langmuir isotherm [16], where the sorbed mass $m_s(h)$ is given by

$$m_s(h) = m_0 \frac{e^{E/kT} h}{1 + e^{E/kT} h}. \quad (1)$$

The Langmuir isotherm is based on the assumption that single molecules are adsorbed at non-interacting sites

with energy of adsorption E . h is the partial pressure of the sorbate, relative to its saturation pressure, and m_0 is the mass adsorbed when the surface is completely covered. To allow direct comparison with experimental results, we must introduce a further parameter δ , where the mass measured is $m_s(h) - \delta$. This accounts for the fact that the water content is not necessarily truly zero when the experimental measurement of “dry mass” is made.

We assume that the total mass adsorbed and inserted can be accurately described by a Langmuir isotherm. There is no solid theoretical reason for applying a Langmuir isotherm to insertion into the solid skeleton, but experimental results suggest that it is at least a reasonable first approximation, in the absence of any superior model. The parameters m_0 , E and δ are determined by fitting the experimentally measured masses at the lowest partial pressures.

When the structure of the solid material intrinsically contains the sorbent, as in the case of water in hardened cement paste, sorption hysteresis extends to the lowest partial pressures, below the pressure at which capillary condensation occurs. To account for this, we let calculated parameter values differ between adsorption and desorption, augmented by a linear increase of mass with partial pressure on adsorption to ensure a closed cycle.

B. Pore filling

Having subtracted the contribution of surface adsorption and intrasolid insertion, the remaining, capillary condensed fluid can be used to assess the pore structure. We assume that, as partial pressure is increased, the process of capillary condensation proceeds according to local thermodynamic considerations, unaffected by the pore network structure. We model the pores as cylinders: the most important geometric property of a pore is its surface area to volume ratio, so the effective radius r of a non-cylindrical pore is the radius of a cylindrical pore with the same surface area to volume ratio. Since pore filling takes place at relatively high sorbate pressure, when there is a more or less complete adsorbed layer on the pore walls, the relevant volume is the volume remaining empty after this adsorption, and the surface area is the surface area of the adsorbed layer.

One way a cylindrical pore can fill is by the adsorbed layer growing in thickness, so that the liquid-vapor interface propagates radially from the outside of the pore to the axis [17]. This will occur when the sorbate pressure is sufficiently high that an infinitesimal increase in layer thickness leads to a decrease in free energy [18] [19]. The pressure at which this condition is satisfied can be calculated by applying the Kelvin equation to the cylindrical liquid-vapor interface:

$$\ln h = -\frac{\gamma v}{kTr}. \quad (2)$$

Here γ is the surface tension of the sorbate and v is the molecular volume. Note that larger pores require higher partial pressure to begin filling. One effect of this is that, once the adsorbed layer begins to grow, it will quickly fill the pore, as the thickening layer decreases the effective pore size.

The other way a pore can fill is through the propagation of a liquid-vapor interface axially from one end of the pore to the other, initiated for example by the adsorbed layer at the end of a closed pore or by a neighboring full pore. In this case, the interface to which the Kelvin equation should be applied is hemispherical, and filling will occur at partial pressure [18] [19],

$$\ln h = -\frac{2\gamma v}{kTr}, \quad (3)$$

which we designate the transition pressure. We assume that the wetting angle is zero, since the pore wall is covered by the adsorbed layer.

It is not immediately obvious which of these descriptions is closer to reality for a particular porous material. Experimental results for primary adsorption and desorption curves are not enough to determine this, as there are sufficient free parameters in any model to fit experimental data using either mechanism. However, since emptying should always occur through axial propagation of the interface, if the interface propagates radially as the pore fills, there will be sorption hysteresis even for an isolated pore [19]. This means that the predicted scanning isotherms depend on which filling mechanism is assumed. Axial filling gives (very slightly) better agreement with experimentally observed scanning isotherms (see section III), so we assume this mechanism henceforth.

When the partial pressure relative to saturation is h , pores of radius up to

$$R(h) = -\frac{2\gamma v}{kT \ln h} \quad (4)$$

will be full. The total capillary condensed mass is therefore

$$m_{\uparrow}(h) = \int_0^{R(h)} v(r) \rho \, dr, \quad (5)$$

where $v(r)$ is the volume density function for pores of effective radius r . Equation 5 allows $v(r)$ to be calculated from measured $m_{\uparrow}(h)$.

This method, and the following treatment of nucleation of the vapor phase in a pore network, are suited to materials with a wide size distribution. Other methods should be used for different cases, such as monodisperse pores with smaller windows connecting them [20].

C. Suppression of nucleation by the network

When sorbate partial pressure is decreased, an isolated pore would empty at its transition pressure, given by the

Kelvin equation (equation 3). A pore in a porous material can also empty at this partial pressure, but only if it is exposed to the liquid-vapor interface. If it is not exposed, the full state remains metastable well below this partial pressure. The water content of a pore thus depends not only on its size and the sorbate partial pressure, but on whether the pore's neighbors are empty. We present two simple models to explain the observed sorption behavior and obtain parameters describing the pore structure: a mean-field percolation model, and a chain model. The percolation model is an obvious first approach to modeling the system, but the low coordination number obtained using this model suggests that the chain model is better for systems with a wide pore size distribution.

1. Percolation model

We begin by assuming that the pore structure is a network of cylindrical pores with length independent of radius, so that the volume of a pore is proportional to the square of its radius. Defining q to be the number fraction of pores for which the ambient partial pressure is below their transition pressure, our aim is to calculate the fraction Q of these pores that is empty. The function $Q(q)$ depends on two important properties of the pore network: connectivity and initial exposure. We use a Bethe lattice of connectivity z , where nodes correspond to pores, as a model of the network: though clearly this is an oversimplification and cannot be taken quantitatively, nevertheless high z implies a highly-connected pore network, while low z implies a network made up of largely independent chains. We define f to be the fraction of all pores exposed to the liquid-vapor interface even when all pores are full, and hence able to empty as soon as the partial pressure drops below each pore's transition pressure.

Any particular pore could have access to the vapor phase via either of two mechanisms. First, the pore could be exposed initially even when the pore network is full: a fraction f of the pores is in this category. Second, it could be connected to the vapor by a neighbor: we define X to be the probability that an individual neighbor provides such a connection. We then can write

$$1 - Q = (1 - f)(1 - X)^z. \quad (6)$$

Taking advantage of the self-similarity of the Bethe lattice, we can further write

$$X = q[f + (1 - f)(1 - (1 - X)^{z-1})]. \quad (7)$$

We solve equation 7 self-consistently to find X , and then use equation 6 to calculate Q .

Comparing the prediction of equation 6 with experimental results, a least-squares fit allows calculation of f and z for various materials. We apply the model to published sorption results for porous silica glass [21]. The best fit gives very small f , 0.01 or less. The connectivity

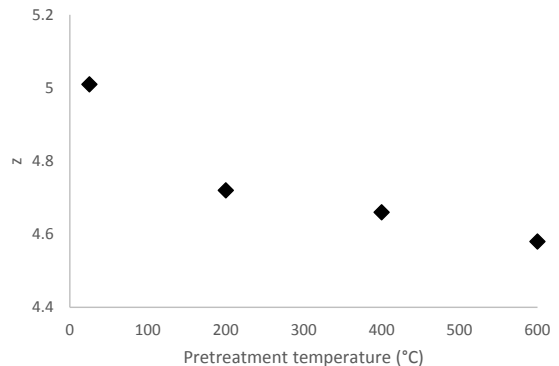


FIG. 1. Variation of connectivity z , calculated using the percolation model to the experimental data of Naono et al. [21], with the pretreatment temperature of the porous silica glass.

parameter z is around 5, and varies with the glass pretreatment temperature (figure 1). Higher temperature pretreatment results in lower connectivity (despite an increase in overall porosity), perhaps because sintering or similar has blocked some connections between pores. In a network with small f and $z \approx 5$, the adsorbed volume varies rapidly with q around the percolation threshold. This is typical for some systems such as porous glass, which have a relatively narrow pore size distribution. This percolation model, which is based on long-established ideas [5, 7, 22] is suitable for such systems.

In contrast, sorption experiments have also been used for many decades to assess the pore structure of materials with a very wide pore size distribution, such as cement paste [23–25] and dental enamel [26]. In these cases, applying the percolation model results in values of f around 0.3 and z less than 2. Since $z = 2$ corresponds to an unbranching, infinite chain of pores, this suggests that the basic idea of an interlinked network of pores is not an accurate model of these systems for the purpose of describing their desorption behavior. We propose an alternate model based on short chains of pores, each exposed at one end.

2. Chain model

The results of the percolation model suggest that a large fraction of pores is exposed to the vapor as soon as partial pressure begins decreasing. This can be understood, in materials with a wide pore size distribution, as being due to prevalent macropores. These macropores are well-known in materials such as cement paste, where they are generally called capillary pores [27]. The largest pores remain empty at all partial pressures, exposing their neighbors to the liquid-vapor interface.

We model the pore network in such a material by a collection of independent chains, assigning each pore to the chain by which it has the shortest connection to an always-empty macropore. We denote the typical number

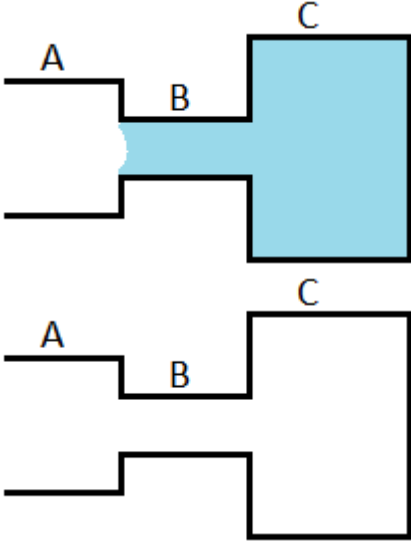


FIG. 2. A schematic illustration of the sequential pore emptying process. At a particular partial pressure, emptying is thermodynamically favorable for both pore A and pore C, but pore C remains full because it has no exposure to a liquid-vapor interface. At a lower partial pressure, pore B empties, leading to the emptying of pore C as well.

of pores in a chain as n , so $f = 1/n$ is the fraction of pores initially exposed to the vapor. f is thus a measure of the prevalence of macropores in the pore network, so high f should be correlated with high permeability. Figure 2 schematically illustrates a chain of three mesopores.

Since a pore is exposed only if all pores between it and the open end of the chain are empty, the total fraction of empty pores is

$$W = \frac{1}{n} \sum_{i=1}^n q^i = f \frac{q(1 - q^{1/f})}{1 - q}, \quad (8)$$

with the definition $W = Qq$.

D. Spinodal decomposition

Equation 8 would define the desorption isotherm were it not for the effect of spinodal decomposition. At sufficiently low partial pressures, a pore even not exposed to the vapor will empty through spinodal decomposition or near-spinodal nucleation, as the filled state becomes unstable to small density perturbations. The importance of this effect to sorption in mesoporous systems has previously been noticed [28], but not included quantitatively in a model that also accounts for the pore network geometry. We model the pressure at which this occurs by

$$h_{sp}(r) = h_{\infty} e^{-\frac{2\gamma v}{r k T}}, \quad (9)$$

where h_{∞} is the partial pressure at which bulk spinodal (or near-spinodal) decomposition occurs. h_{∞} is a pa-

rameter in the model, with a value that depends on sorbate and temperature but not on the sorbent. We can then define a quantity $q^* < q$ to be the fraction of pores for which the applied partial pressure h is below their spinodal transformation pressure h_{sp} : these pores will be empty regardless of their exposure to the vapor region.

The presence of these definitely empty pores increases the effective f of the pore network. Since a spinodally transformed pore will (a) leave the number of exposed pores unchanged if it is at the open end of a chain, (b) increase the number by one if it is at the back end, or (c) increase the number by two if it is anywhere else, the effective f for a system with spinodally transformed pores is

$$\tilde{f} = f + q^*[f + (1 - 2f)2] = f + q^*(2 - 3f). \quad (10)$$

We then define

$$\tilde{q} = \frac{q - q^*}{1 - q^*}, \quad (11)$$

the equivalent of q but for the network consisting only of the pores that have not spinodally transformed. After calculating \tilde{Q} from \tilde{f} and \tilde{q} exactly as we calculated Q from f and q , the total capillary condensed mass is

$$m_{\downarrow}(h) = \int_0^{R(h)} v(r)\rho \, dr + (1 - \tilde{Q}) \int_{R(h)}^{R^*(h)} v(r)\rho \, dr \quad (12)$$

where

$$R^*(h) = -\frac{2\gamma v}{kT \ln h/h_{\infty}}, \quad (13)$$

the effective radius above which pores have spinodally emptied. Of course, if h is above h_{∞} , quantities with tildes are equal to their untilded counterparts and R^* is infinity.

III. COMPARISON WITH EXPERIMENT

We apply equations 1, 5 and 12 to published sorption isotherms, using least squares fits to determine parameter values. Low pressure sorption data give values of $e^{E/kT}$ of 1 for nitrogen on carbon nanotubes at 77 K, 18 for water on hardened cement paste at 296 K, 7 for water on dental enamel at 298 K and 8 for water on dental enamel at 323 K. Since the assumption of Langmuir adsorption oversimplifies the situation because it ignores insertion within the solid material, these values cannot be directly converted into sorption energies. Nevertheless, higher values should correspond to more hydrophilic sorbents.

Figure 3 provides some examples of comparisons between the results of the model and experimental sorption isotherms [29] [30] [26]. The pore size distribution is calculated directly from the adsorption isotherms. Figure 4 shows the calculated pore size distribution for these materials. The radii of the carbon nanotubes was measured

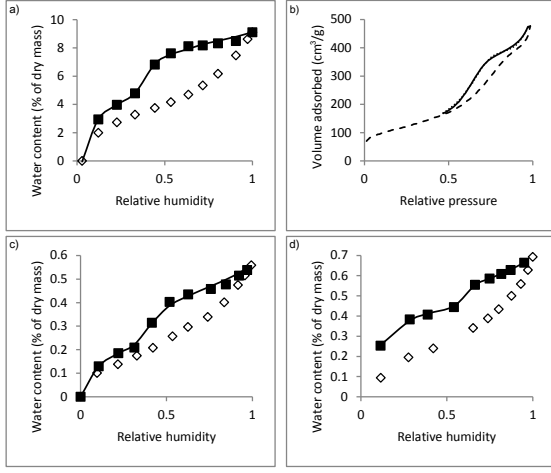


FIG. 3. Desorption isotherms calculated using the model of this work (solid lines), along with experimental adsorption (open diamonds or dashed line) and desorption (solid squares or dotted line) isotherms for a) water in hardened cement paste at 296 K [29], b) nitrogen in carbon nanotubes at 77 K [30], c) water in dental enamel at 298 K [26] and d) water in dental enamel at 323 K [26].

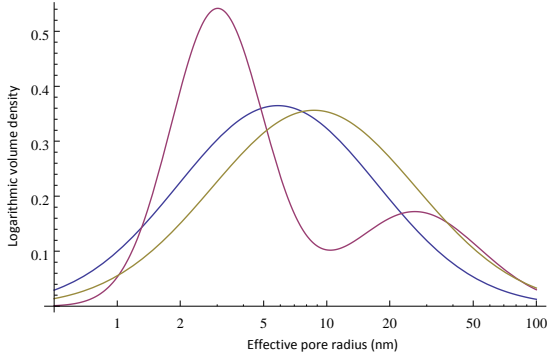


FIG. 4. Logarithmic volume density function for carbon nanotubes, with radii measured by TEM to be between 2 and 3 nanometers (purple) [30], as well as for cement paste (brown) [29] and dental enamel (blue) [26].

by transmission electron microscopy (TEM) to be between 2 and 3 nanometers [30]. To avoid artificial jaggedness in the plotted probability density function, the best fit log-normal distribution is shown (two log-normal distributions in the case of carbon nanotubes, which shows a distinct bump in the adsorption isotherm). Since the model equations for desorption are based on the cumulative density function, this smoothing was not needed for calculation of the theoretical desorption isotherms.

Values of f calculated from the desorption isotherm for these materials, along with some other samples of cement paste [29], are presented in table I.

The calculated value of f gives fundamental information about the pore structure. In the case of cement paste, high porosity is correlated with high f . This agrees with the observation of Kumar et al. [31] that the overall

TABLE I. Initial fraction of exposed pores, calculated by applying the model presented here to a variety of published experimental data [30] [29] [26]. Porosities are approximate.

Material	Porosity	f
Cement paste	0.34	0.29
Cement paste	0.31	0.26
Cement paste	0.24	0.21
Cement paste	0.19	0.20
Carbon nanotubes	0.7	0.2
Dental enamel	0.01	0.2

porosity alone explains most of the variation in sorption behavior between different samples of cement paste. On the other hand, there is no obvious correlation between porosity and f when comparing different materials: materials with very different porosity have similar f .

The principles of the model can be applied directly to the case of scanning isotherms, where the partial pressure is cycled over some subsection of the possible range.

If the decrease in partial pressure is halted at h_{min} and the partial pressure then increased to h , the total sorbed mass will be

$$m_{\uparrow scan}(h) = \int_0^{R(h)} v(r) \rho \, dr + [1 - \tilde{Q}(h_{min})] \int_{R(h)}^{R^*(h_{min})} v(r) \rho \, dr,$$

since the water that was in a meta-stable liquid state at the lowest partial pressure remains in this state.

If the increase in partial pressure is halted at h_{max} and the partial pressure then decreased to h , the total sorbed mass can be calculated using equation 12, but using the smaller of $R^*(h)$ and $R(h_{max})$ in place of $R^*(h)$, i.e. the radius of the largest pores that could be filled. The value of q^* is likewise the fraction of pores larger than this radius.

Figure 5 compares the model with experimental scanning isotherms for dental enamel [26]. For accurate predictions, the turning point needs to be fixed by mass rather than partial pressure when it lies in a region where mass changes rapidly with partial pressure.

Various differences can be observed between sorption isotherms for the same sorbate and sorbent at different temperatures: see, for instance, the lower half of figure 3. Relatively small changes result from the explicit dependence of equation 3 on temperature and the change in surface tension with temperature. A larger change arises, at least in the case where water is used as the sorbate, because increasing temperature increases the quantity of water that can be removed from within the structure of the sorbate itself. For this reason, calculated values of E , m_0 and δ are not transferable between temperatures.

Most interesting is the variation of h_∞ , the partial pressure at which spinodal decomposition occurs in the largest pores, with temperature. Figure 6 plots h_∞ as

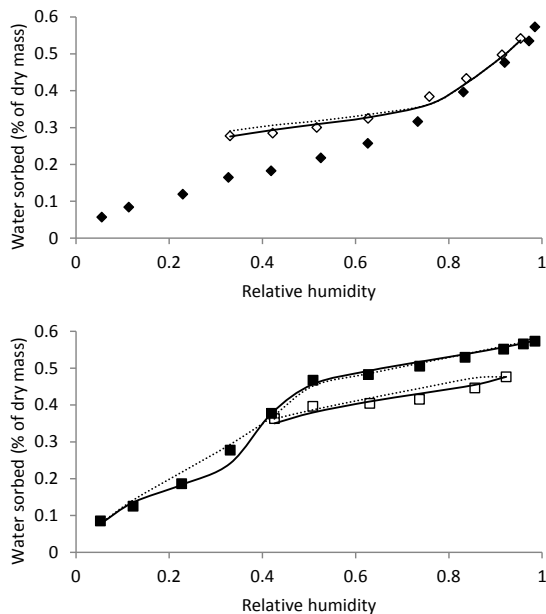


FIG. 5. a) Scanning adsorption isotherm calculated using the model of this work (solid line), and using the same model but assuming radial filling (dotted line), along with experimental primary (solid diamonds) and scanning (open diamonds) adsorption isotherms for water in dental enamel at 298 K [26]. No calculated primary adsorption isotherm is shown because this isotherm is an input to the model. b) Primary and scanning desorption isotherms calculated using the model of this work (solid lines), and using the same model but assuming radial filling (dotted lines), along with experimental primary (solid squares) and scanning (open squares) desorption isotherms for water in dental enamel at 298 K [26].

a function of the reduced temperature $\tau = T/T_c$, where T_c is the critical temperature of the bulk fluid. At the critical temperature, the first order liquid-vapor phase transition disappears, so h_∞ must go to 1. The points calculated by applying the model to experimental data are consistent with a smooth curve ending at (1,1). Simple model equations of state predict a universal form of this curve, from which the interaction strength is absent when pressure is expressed relative to saturation pressure and temperature relative to the critical temperature. The regular solution model predicts

$$h_\infty = \frac{e^{-2\sqrt{1-\tau}/\tau}(1 + \sqrt{1-\tau})}{1 - \sqrt{1-\tau}}, \quad (14)$$

and a numerical result can be obtained for a van der Waals gas.

IV. CONCLUSIONS

The interpretation of sorption-desorption isotherms of mesoporous materials presents several challenges. The model presented here explains many of the observed fea-

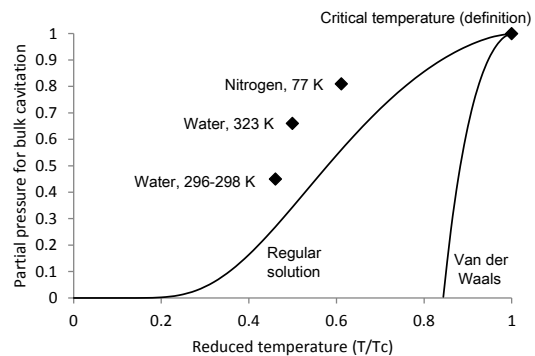


FIG. 6. h_∞ calculated using the model of this work (points), along with theoretical values from the regular solution and van der Waals models.

tures, though there remains room for further development.

The hysteresis is identified as resulting from sorbate in large pores located behind smaller pores remaining condensed due to the absence of a liquid-vapor interface, and the resulting lack of a decreasing free energy path to the empty state. The development here of a simple model relating macroscopic sorption behavior to microstructure should contribute to the design of materials for applications such as moisture buffering [32], and the understanding of the dependence of thermal conductivity on water content [33].

The model makes use of the observed hysteresis, which has presented difficulties in interpretation of isotherms, to extract not only a pore size distribution but also a measure of the connectivity of the pore structure. Since connectivity plays a vital role in determining the transport properties of a material [34, 35], it would be very interesting for future research to examine the relationship between f and the permeability of a material.

The model presented here has the potential to contribute to transport modeling not only through its assessment of connectivity, but also by identifying and explaining the hysteresis in the sorbed mass as a function of local sorbate chemical potential. Existing models of transport in porous materials do not account for this hysteresis, nor even treat transport from a thermodynamic basis by relating flux to the gradient of chemical potential, but simply define an effective diffusivity $D(S)$ [36, 37] by

$$\frac{\partial S}{\partial t} = \nabla \cdot [D(S) \nabla S], \quad (15)$$

where S is the local saturation of sorbate, or equivalent. Although this can give a qualitative idea of the conditions under which transport is faster or slower, the transport rate must be connected to chemical potential gradients though a model such as the one presented here in order for transport mechanisms to be understood. Such an understanding will assist in the design of materials with desired transport properties. This is particularly important because degradation and contamination in concrete

[38–40] and many other materials [41, 42] rely on the transport of water and of ions dissolved in the water.

The model also identifies the significant bump in the desorption isotherm, around 40% relative pressure in the case of water at 25 °C, as being due to spinodal decomposition. The pressure at which this bump is located varies with temperature in a reasonable way, though data are limited. This model therefore provides significant progress towards a complete understanding of sorption-desorption isotherms in materials with a wide pore size distribution.

One important ingredient of our model is that it accounts for the insertion of sorbate into the solid skeleton, and particularly the hysteresis in this process. However, we do not attempt to explain or predict this hysteresis. Since the insertion process is highly dependent on the chemistry of the sorbate and sorbent, a more detailed, material-specific model, such as one based on atomic-level simulation, is needed to approach a quantitative explanation. Nevertheless, a simple subtraction of an inserted mass calculated by fitting a smooth curve works quite well, when it is the sorption in mesopores that is of interest. In order to understand the mesopore structure in the absence of a model of insertion, it could be useful to ensure that sorbate pressure always remains above that at which sorbate is removed from the solid material.

In the case of water in cement paste, this value is around 20% relative humidity.

Another unresolved question is the importance of single-pore hysteresis. If the path traversed by the liquid-vapor surface is different on filling and emptying, these processes will occur at different partial pressures [17]. The assumption of this work, that hysteresis resulting from this difference is insignificant and network effects dominate, provides a better prediction of scanning isotherms than the opposite assumption that single-pore hysteresis dominates and network effects are unimportant. It is reasonable to believe that in fact both mechanisms contribute to the observed hysteresis, but a more complete range of scanning isotherms is needed to assess their relative importance.

ACKNOWLEDGMENTS

The authors acknowledge useful discussions with the members of the Dome collaboration and G. Sant. This work was supported by the CSHub@MIT with sponsorship provided by the Portland Cement Association (PCA) and the Ready Mixed Concrete (RMC) Research & Education Foundation, and by the National Science Foundation via an EAGER Collaborative Grant #1153509.

-
- [1] A. C. A. Muller, K. L. Scrivener, A. M. Gajewicz, and P. J. McDonald, *The Journal of Physical Chemistry C* **117**, 403 (2013).
 - [2] K. S. W. Sing, *Pure and Applied Chemistry* **57** (1982).
 - [3] P. T. Tanev and L. T. Vlaev, *Journal of colloid and interface science* (1993).
 - [4] P. I. Ravikovitch and A. V. Neimark, *Langmuir*, 9830 (2002).
 - [5] G. Mason, *Proceedings of the Royal Society of London. A* **390**, 47 (1983).
 - [6] G. Mason, *Proceedings of the Royal Society A: Mathematical, Physical and Engineering Sciences* **415**, 453 (1988).
 - [7] M. Parlar and Y. C. Yortsos, *Journal of colloid and interface science* **124**, 162 (1988).
 - [8] N. A. Seaton, *Chemical Engineering Science* **46**, 1895 (1991).
 - [9] F. A. L. Dullien, *Porous Media Fluid Transport and Pore Structure*, 2nd ed. (Academic Press, San Diego, 1992) pp. 22–28.
 - [10] L. Bertolini, B. Elsener, P. Pedferri, and R. Polder, *Corrosion of Steel in Concrete Prevention, Diagnosis, Repair* (Wiley-VCH, Weinheim, 2004) pp. 21–48.
 - [11] S. Choi, J. H. Drese, and C. W. Jones, *ChemSusChem* **2**, 796 (2009).
 - [12] F. Javadpour, D. Fisher, and M. Unsworth, *Journal of Canadian Petroleum Technology* **46**, 55 (2007).
 - [13] I. G. Richardson, *Cement and Concrete Research* **34**, 1733 (2004).
 - [14] I. Richardson, *Cement and Concrete Research* **38**, 137 (2008).
 - [15] Z. P. Bazant and M. Z. Bazant, *Journal of the Mechanics and Physics of Solids* **60**, 1644 (2012).
 - [16] I. Langmuir, *Journal of the Franklin Institute* **38**, 2221 (1917).
 - [17] F. Celestini, *Physics Letters A* **228**, 84 (1997).
 - [18] L. H. Cohan, *Journal of the American Chemical Society* **60**, 433 (1938).
 - [19] J. C. P. Broekhoff and J. H. De Boer, *Journal of Catalysis* **9**, 8 (1967).
 - [20] K. A. Cychosz, X. Guo, W. Fan, R. Cimino, G. Y. Gor, M. Tsapatsis, A. V. Neimark, and M. Thommes, *Langmuir* **28**, 12647 (2012).
 - [21] H. Naono, R. Fujiwara, and M. Yagi, *Journal of Colloid and Interface Science* **76**, 74 (1980).
 - [22] G. Mason, *Journal of Colloid and Interface Science* **88**, 36 (1982).
 - [23] R. F. Feldman and P. J. Sereda, *Journal of Applied Chemistry* **14**, 87 (1964).
 - [24] D. Quenard and H. Sallee, *Materials and Structures* **25**, 515 (1992).
 - [25] R. M. Espinosa and L. Franke, *Cement and Concrete Research* **36**, 1954 (2006).
 - [26] R. T. Zahradnik and E. C. Moreno, *Arcs oral Biol.* **20**, 317 (1975).
 - [27] T. Powers, *Journal of the American Ceramic Society* **41**, 1 (1958).
 - [28] M. Z. Bazant and Z. P. Bazant, *Journal of the Mechanics and Physics of Solids* **60**, 1660 (2012), arXiv:arXiv:1111.4759v1.

- [29] V. Baroghel-Bouny, *Cement and Concrete Research* **37**, 414 (2007).
- [30] E. Frackowiak and F. Béguin, *Carbon* **39**, 937 (2001).
- [31] A. Kumar, S. Ketel, K. Vance, T. Oey, N. Neithalath, and G. Sant, *Transport in Porous Media* (2014), 10.1007/s11242-014-0288-5.
- [32] O. F. Osanyintola and C. J. Simonson, *Energy and Buildings* **38**, 1270 (2006).
- [33] M. Jerman and R. Černý, *Energy and Buildings* **53**, 39 (2012).
- [34] C. Hall and M. Raymond Yau, *Building and Environment* **22**, 77 (1987).
- [35] C. Hall, W. D. Hoff, S. C. Taylor, M. A. Wilson, B.-G. Yoon, H.-W. Reinhardt, M. Sosoro, P. Meredith, and A. M. Donald, *Journal of Materials Science Letters* **14**, 1178 (1995).
- [36] N. S. Martys and C. F. Ferraris, *Cement and Concrete Research* **27**, 747 (1997).
- [37] V. Baroghel-Bouny, *Cement and Concrete Research* **37**, 438 (2007).
- [38] P. Faucon, F. Adenot, J. F. Jacquinot, J. C. Petit, R. Cabrillac, and M. Jorda, *Cement and Concrete Research* **28**, 847 (1998).
- [39] E. Samson, J. Marchand, and J. J. Beaudoin, *Cement and Concrete Research* **30**, 1895 (2000).
- [40] F. P. Glasser, J. Marchand, and E. Samson, *Cement and Concrete Research* **38**, 226 (2008).
- [41] J. Šimnek and D. L. Suarez, *Water Resources Research* **30**, 1115 (1994).
- [42] K. U. Mayer, E. O. Frind, and D. W. Blowes, *Water Resources Research* **38**, 13 (2002).